The effect of combustor width on continuous rotating detonation wave fueled by ethylene

Haoyang Peng[1], Weidong Liu[1], Shijie Liu[1]
[1]Science and Technology on Scramjet Laboratory, National University of Defense Technology, Changsha, 410073, China

1 Introduction

Continuous Rotating Detonation (CRD) Engine has huge potential benefits due to its higher thermodynamic efficiency, faster heat release rate and simpler structure. Extensive studies of CRD fueled by hydrogen in experiment and numerical simulation have been accomplished. Kerosene may be the ideal fuel for CRD propulsive application. However, it is difficult to obtain the kerosene CRD at present due to its low chemical activity. Ethylene is an excellent choice of the transition from hydrogen to kerosene, because its chemical activity is comparatively active in hydrocarbon fuel and its combustion flame is luminous enough for optical observation.

The majority of CRD Engine fueled by ethylene has been investigated in the USA at present. Richard Dyer et al. [1] conducted successful experiment fueled by ethylene and bottled air with 24.8% oxygen content. They summarized the operating domain and found that all the propagation modes were single wave. Jarred Wilhite et al. [2] conducted experiment with ethylene and air. Successful cases were seen to occur for only mass flow rate of 0.2 kg/s and 0.3 kg/s and equivalence ratios (ERs) in the range of $0.85< \emptyset < 1.34$. Kevin Y. Cho et al. [3] focused on the ethylene detonation waves (DWs) structure in an annular combustor by using OH* chemiluminescence imaging. In their images, a low temperature region between the DW and the oblique shock was observed. Specially, the stand-off distance and the wave height of DWs were quantitatively measured.

Bykovskii et al. [4] considered that combustor width should be larger than a critical value for the CRD realization and the critical value is the half of detonation cell size. The detonation cell sizes of stoichiometric hydrogen-air, ethylene-air and methane-air under normal temperature and atmospheric pressure are 8 mm, 25.68 mm and 350 mm, respectively [5,6]. The cell size of hydrocarbon is much larger than that of hydrogen. So the combustor width may be a key factor for hydrocarbon CRD tests. This paper mainly focuses on the effects of combustor widths on the ethylene CRD. Series of test have been carried out by changing the ERs under different combustor configurations, and the operating domain of ethylene CRD is summarized. Based on the high frequency pressure and optical observations, the propagation characteristics of ethylene CRD are also detailed.

2 Experimental System

At present, many flowfield diagnosis technologies cannot be applied to CRD Engine due to its annular channel combustion. The curve glass installed on annular combustor causes refraction and image distortion. On contrast of conventional annular combustor, a racetrack configuration is proposed, which contains two straight sections and two semicircles. A schematic diagram of the optically-accessible racetrack combustor is illustrated in Fig.1. The plain quartz glass installed in straight section can avoid the image distortion caused by curve glass. Propellants are provided via a slit-orifice collision spray pattern [7]. The oxidizer in this test is the mixture of air and oxygen, with the oxygen mass ratio of 35%, labeled as oxygen-enriched air. The oxidizer is injected through convergent-divergent slit, and its throat width is 0.4 mm. The outer wall of the slit is straight and the configuration is designed for upstream observation. Ethylene is injected through 90 orifices distributed uniformly along the inner body, and the injection angle is 45 degree. Two sets of fuel injectors are used and the diameters are 0.6 mm and 0.8 mm, respectively. By substituting the inner body, several combustor widths can be obtained, including 8 mm, 12 mm, 15 mm, 20 mm and hollow chamber (hc). A pre-detonator connected tangentially to the combustor is used for detonation initiation and its propellants are hydrogen and oxygen.

The installation positions of quartz windows and transducers are marked in Fig.2. To detect the high frequency pressure in the detonation combustor, 4 PCB sensors are installed on the outer wall of the combustor. PCB2 and PCB3 are installed at the same axial location and their circumferential angle is 45 degree. The radius of semicircle is 40 mm and the length of straight section is also 40 mm. And the length of combustor is 130 mm. The optical observation window is a rectangle, which is 131 × 40 mm in size, and its upstream boundary is 40 mm away from the fuel injector location. The images are acquired by the Photron Fast Camera SA-X at a frame rate of 72 kHz, with the resolution of 640 × 256 pixels.

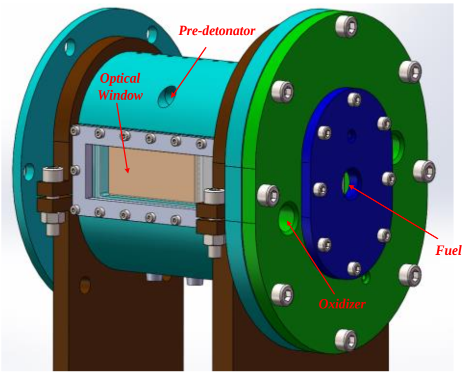

Fig.1 Schematic diagram of the optically-accessible racetrack combustor

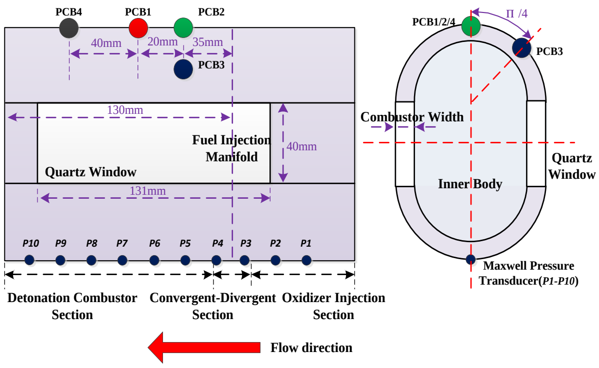

Fig.2 The installation positions of quartz windows and transducers

3 Results and Discussions

Series of CRD tests with different combustor width, injection schemes and ERs are conducted. The oxidizer mass flow rate is relatively stable, in the range of 280g/s-315g/s. Different ERs are achieved by changing the ethylene mass flow rate.

3.1 Operating Domain

Operating domain maps of CRD fueled by ethylene and oxygen-enriched air on two injection schemes are shown in Fig.3. The symbol ‘O’ stands for successful case and symbol ‘X’ stands for unsuccessful case. The region between lean limit and rich limit stands for the operating domain of ER, which is showed as the strip below coordinate system.

When the combustor width is 8 mm, CRD cannot be achieved with the fuel injector diameter of 0.8 mm as shown in Fig.3b, and it can be obtained with the fuel injector diameter of 0.6 mm as shown in Fig.3a. Its operating ER domain is just 0.93-0.96. However, its lean limit and rich limit have overlap which means the domain is near the operating boundary. On contrast of hydrogen CRD which can be achieved on 5 mm or 8 mm wide combustor with large operating domain, CRD fueled by ethylene is hardly achieve on corresponding combustor. A relatively larger combustor width is needed for ethylene CRD. When the combustor width increases to 12 mm, the operating domain enlarges rapidly. However, the operating domain is relatively consistent with the further increase of the combustor width, even to a hollow chamber. The operating domain seems the largest when the combustor width is 15 mm. Fig.3b also shows the similar feature with 0.8 mm diameter injector.

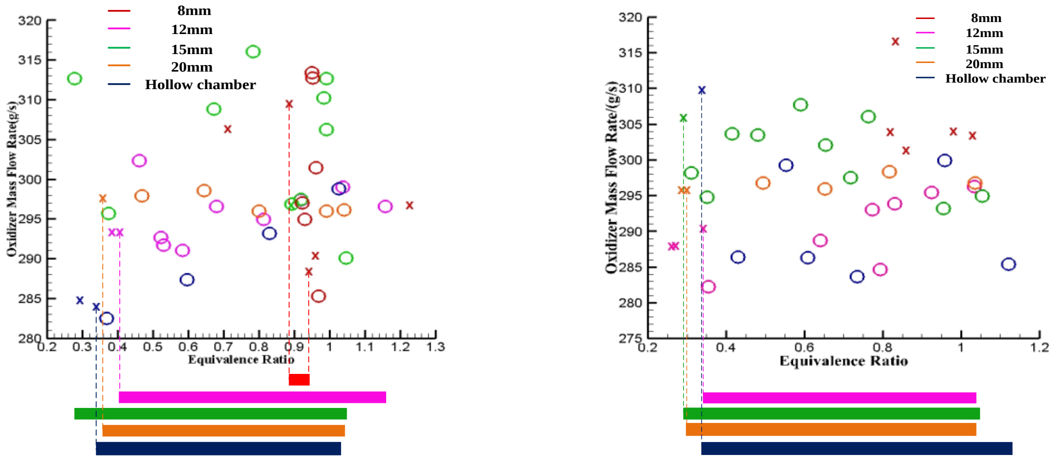

Fig.3 Operating domain maps on different diameter injectors
(Left: (a) injector diameter =0.6 mm; Right: (b) injector diameter =0.8 mm)

3.2 Propagation characteristics and flowfield structure

In the CRD series tests, combustor width has effect on propagation characteristics as well as operating domain. CRD Waves propagate mostly as two wave in hetero-rotating mode in combustor with inner body, while they propagate mostly as single wave or two wave in homo-rotating mode in hollow chamber. The propagation modes are different from the experiment of Richard Dye et al. [1], all of whose propagation modes are single wave. Typical operating conditions and corresponding combustor configurations are listed in Table 2.

Table 2 Operating condition and combustor configuration

Test No.	Combustor configuration	Oxidizer mass flow rate（g/s）	Propagation Mode	ER
#1	8 mm-90×0.6mm	312.71	Two wave in hetero-rotating mode [8]	0.951
#2	12mm-90×0.6mm	298.97	Two wave in hetero-rotating mode	1.038
#3	15mm-90×0.6mm	290.06	Two wave in hetero-rotating mode	1.050
#4	20mm-90×0.6mm	294.64	Two wave in hetero-rotating mode	1.035
#5	hc -90×0.6mm	298.81	Single wave	1.027

Test #4 and Test #5 are typical two wave in hetero-rotating mode and single wave mode, respectively. The whole time of CRD is longer than 200 ms, during which detonation can propagate steadily more than 500 circles. After high-pass filter processing, the local views of high frequency pressures are shown in Fig.4 and its PCB signals show strong repeatability. For PCB2, the instantaneous frequency is acquired by $f_i = 1/\Delta T_i$, where f_i is instantaneous frequency and ΔT_i is the time interval of continuous pressure peak, as labeled in Fig.4. The average frequency is calculated by all steady periods data, as shown in Eq.(1), where N is the number of period. The average propagating velocity can be calculated by Eq.(2), where D_{out} is outer diameter and L is the length of straight section. The average propagating velocity and Fast Fourier Transformation (FFT) of Test #4 and Test #5 are shown in Fig.5 and Fig.6, respectively.

$$\bar{f} = \frac{\sum_{i=1}^{N} f_i}{N} \tag{1}$$

$$v = (\pi D_{out} + 2L)\bar{f} \tag{2}$$

As shown in Fig.4(a), the propagation mode is two wave in hetero-rotating mode. DW1 propagates through PCB3 clockwise and the transmitted shock wave, namely, DW2', propagates through PCB3 anticlockwise after collision. The time interval of two DWs recorded by PCB3 is small, beacuse the collision point is close to PCB3. In Fig.4(b), the propagation mode is single wave. There always are relatively lower peaks following the main peak. The propagation direction is from PCB2 to PCB3. For Test #5, the average propagation frequency is 4.98 kHz and the average rotating velocity is 1647.92 m/s. On contrast, the average propagation frequency is 3.55 kHz and the average rotating velocity is 1175.20 m/s in Test #4. More specific, the average propagating velocity is 1063.78 m/s on the intermediate diameter location.

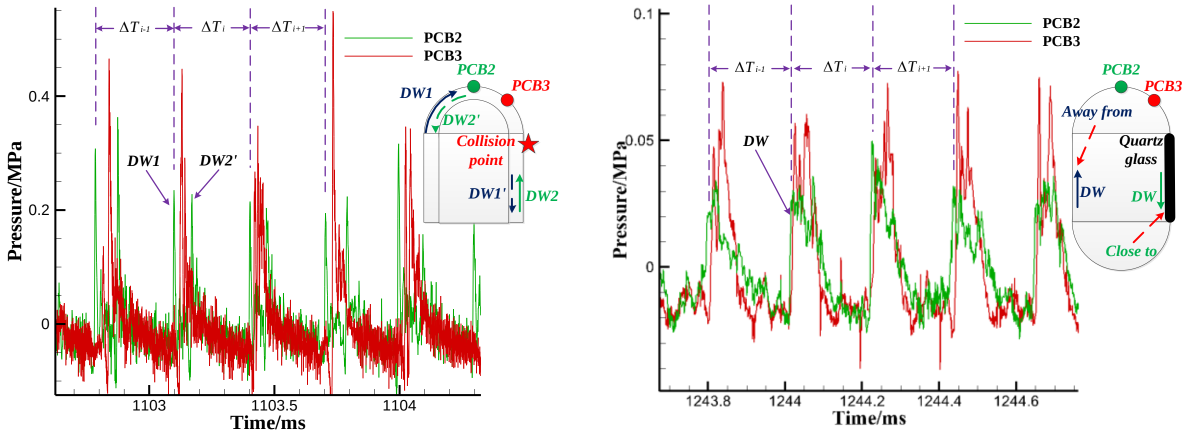

Fig.4 Local view of high frequency pressure results with different combustor configurations (Left: (a) Test #4; Right: (b) Test #5)

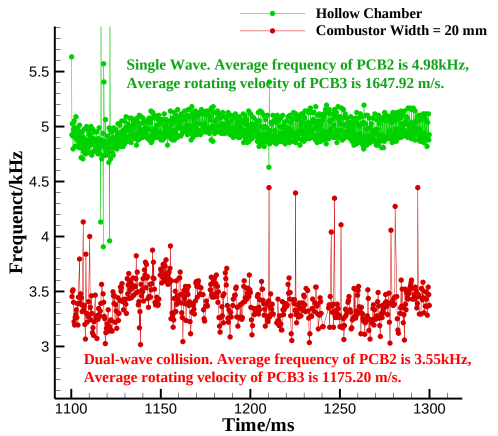

Fig.5 Average propagating velocity results

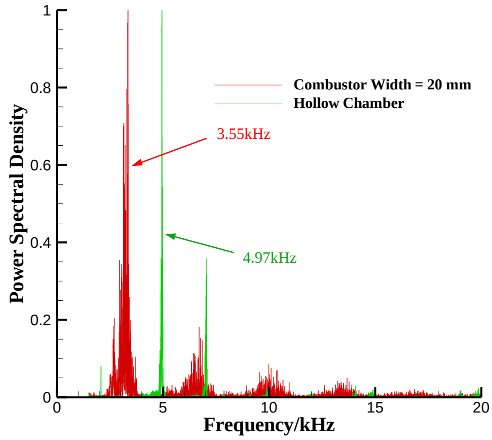

Fig.6 Fast Fourier Transformation results

For futher understanding of CRD Wave propagation characteristics and flowfield structure, optical observation images are acquired. The continuous images of Test #4 and Test #5 are shown in Fig.7 and Fig.8, respectively. To show the most luminous area moving obviously, the propagating tracks of DW are marked by red lines. In Fig.7, the CRD waves in Frame1-2 are captured propagating from bottom to top, which is exactly labeled as DW2 in Fig.4(a). In Frame3 of Fig.7, two wave in hetero-rotating mode process is also captured distinctly and intuitively. There are two distinct DWs with clear boundary, but specific propagation direction of each DW and specific moment after or before collision are still unclear. So the collision point is just marked in Frame3. It is self-evident that the combustion during the collision period is luminous and intense. After collision, the DW1' keeps propagating with relative high intensity in Frame 4.

In the hollow chamber, images of CRD Waves are also acquired in Fig.8. Without the inner body, the DW can be recorded twice in a period, illustrated in the schematic diagram of Fig.4b. The combustion flame in optically-accessible area exists for long time, but the move of flame is still clear and distinguishable. In Frame 3-5, a DW propagating from top to bottom close to quartz glass is captured. When the DW propagates to the other side, a DW propagating from bottom to top away from quartz glass is also captured and marked with dotted line in Frame 10-12. The dotted line in Frame11 and the solid line in Frame 3 are at the similar position compared in the figure, so the CRD Wave is considered to propagate the half distance of combustor perimeter. Based on the frame rate, geometry size and image scale, the velocity of the CRD Wave is calculated as 1192 m/s, which agrees generally with the average propagating velocity measured by PCB. It indicates that the inducing shock wave and the combustion flame are coupled with each other.

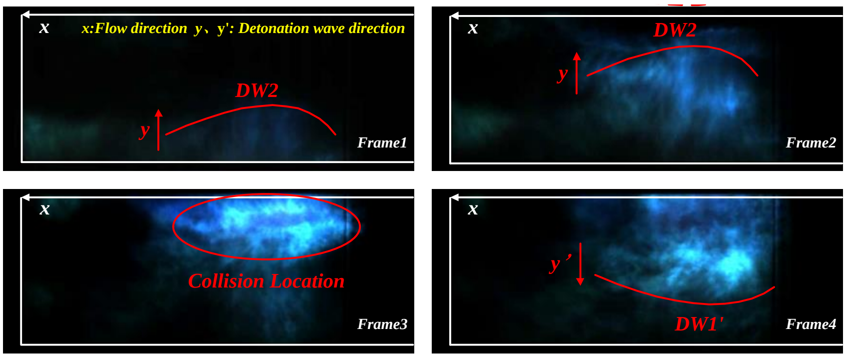

Fig.7 Images of two wave in hetero-rotating mode in Test #4

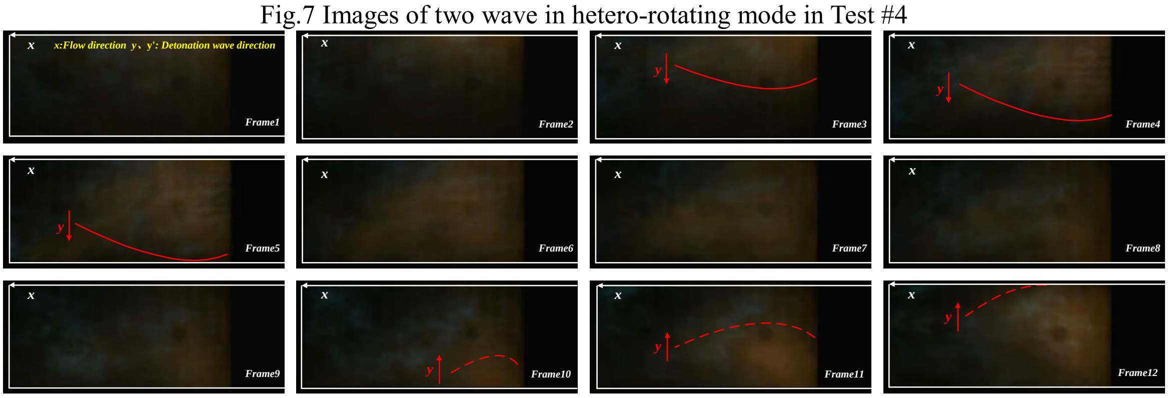

Fig.8 Images of single wave in Test #5

3.1 Propagation stability

Standard deviation and relative standard deviation are quantitative criterions to analyze the effect of combustor width on stability of CRD Wave. The instantaneous propagating frequencies during steady phase in test are chosen as samples. The calculation methods are shown as Eq. (3) and Eq. (4).

$$S = \sqrt{\frac{\sum_1^N (f_i - f_{av})^2}{N-1}} \tag{3}$$

$$\mu = \frac{S}{f_{av}} \tag{4}$$

Where f_{av} is average propagating frequency during steady phase, S is standard deviation and μ is relative standard deviation. The series of tests in Table 2 are calculated and recorded, as shown in Fig.9.

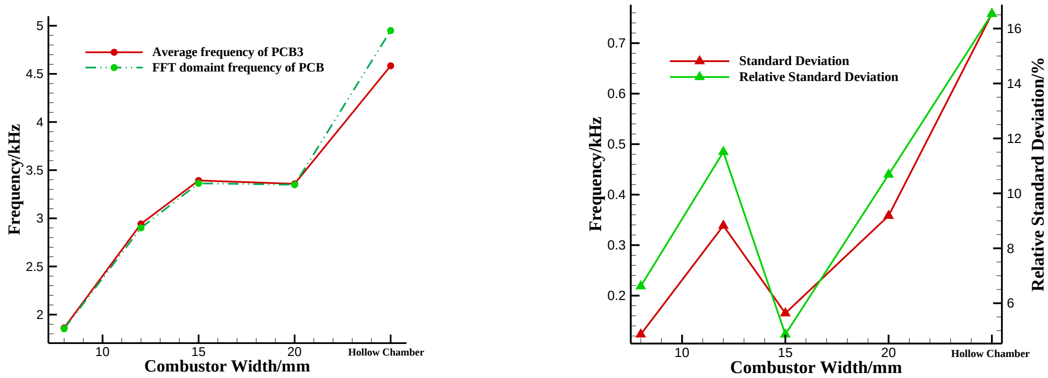

Fig.9 Effect of combustor width on frequency and stability

(Left: (a) Frequency; Right: (b) Standard deviation and relative standard deviation)

As shown in Fig.9(a), average frequency and FFT domain frequency both increase along with combustor width increasing to 15 mm. And there is little frequency difference between 15 mm and 20 mm wide combustor. When inner body is removed, there is rapid frequency increase because of the transformation from two wave in hetero-rotating mode to single wave. In Fig.9(b), CRD Wave in 15 mm wide combustor is the steadiest and in hollow chamber is the most unstable. Considering the operating domain and propagation stability, 15 mm wide combustor is the best choice for ethylene CRD in this test.

4 Conclusions

CRD fueled by ethylene is achieved in optically-accessible racetrack combustor. By varying the combustor width, operating domain, propagation characteristics, flowfield structure and stability are investigated. Ethylene CRD can be achieved on larger width combustor compared with CRD fueled by hydrogen due to its relatively bigger detonation cell size. In the experiments, CRD Waves propagate mostly as two wave in hetero-rotating mode in combustor with inner body, while they propagate mostly as single wave or two wave in homo-rotating mode in hollow chamber. Based on the high frequency pressure and optical observations, both the propagation modes are detailed. The rotating velocities of the inducing shock wave and combustion flame are calculated by PCB results and optical observations respectively, and they agree generally with each other. It indicates that the inducing shock wave and the combustion flame are coupled with each other. Considering the operating domain and propagation stability, 15 mm wide combustor is the best choice for ethylene CRD in this test. The study will improve the combustor design of CRD Engine fueled by hydrocarbon fuels and enhance the understanding of flowfield structure and flame dynamics of CRD Waves.

Acknowledgements

This work is supported by the National Natural Science Foundation of China through Grant No. (91541103 and 51476186).

References

[1] Dyer R, Naples A, Kaemming T, Hoke J, Schauer F. (2012). Parametric testing of a unique rotating detonation engine design. 50th AIAA. Nashville, Tennessee.

[2] Wilhite J, Driscoll R, St George A, Anand V, J. Gutmark E. (2016). Investigation of a Rotating Detonation Engine using Ethylene-Air Mixtures. 54th AIAA, California.

[3] Cho KY, Codoni JR., Rankin BA, Hoke JL, Schauer FR. (2016). High-Repetition-Rate Chemiluminescence Imaging of a Rotating Detonation Engine. 54th AIAA, California.

[4] Bykovskii FA, Zhdan SA, Vedernikov EF. (2006). Continuous Spin Detonation. J Propulsion Power, 22 (6): 1204-1216.

[5] Ciccarelli G, Ginsberg T, Boccio J, Finfrock C, Gerlach L, Tagawa H, and Malliakos A. (1997). Detonation cell size measurements in high-temperature hydrogen-air-steam mixtures at the bnl high-temperature combustion facility. (No. NUREG/CR--6391; BNL-NUREG--52482). Nuclear Regulatory Commission, Washington, DC (United States). Div. of Systems Technology; Brookhaven National Lab., Upton, NY (United States); Nuclear Power Engineering Corp., Tokyo (Japan).

[6] Beeson HD, Clenagan Mc, Bishop CV, Benz FJ, Pitz WJ, Westbrook CK, and Lee JHS. (1991). Detonability of hydrocabon fuels in air. Astronaut. Aeronaut. 133:19.

[7] Lin W, Zhou J, Liu SJ, Lin ZY, Zhuang FC. (2015). Experimental study on propagation mode of H2/Air continuously rotating detonation wave. Int. J. Hydrogen Energy 40:1980.

[8] Wang C, Liu WD, Liu SJ, Jiang LX, Lin ZY. (2015). Experimental investigation on detonation combustion patterns of hydrogen/vitiated air within annular combustor. Experimental Thermal and Fluid Science 66: 269.